Electrical and Thermal Interface Conductance of Carbon Nanotubes Grown under Direct Current Bias Voltage

Placidus B. Amama,*,† Chun Lan,‡ Baratunde A. Cola,†,§ Xianfan Xu,†,§ Ronald G. Reifenberger,†,‡ and Timothy S. Fisher*,†,§

Birck Nanotechnology Center, School of Mechanical Engineering, and Department of Physics, Purdue University, West Lafayette, Indiana 47907

Received: August 26, 2008; Revised Manuscript Received: October 16, 2008

The electrical resistance of individual multiwalled carbon nanotubes and the thermal interface resistance of nanotube arrays are investigated as functions of dc bias voltage used during growth. Nanotubes were grown from Fe_2O_3 nanoparticles supported on $Ti/SiO_2/Si$ substrates by microwave plasma chemical vapor deposition (MPCVD) under dc bias voltages of −200, −100, 0, +100, and +200 V. Electrical resistances of individual nanotubes were obtained from $I-V$ measurements of randomly selected nanotubes, while thermal interface resistances of nanotube arrays were measured using a photoacoustic technique. The study reveals that individual nanotubes and nanotube arrays grown under positive dc bias voltage (+200 V) show significant increases in their electrical and thermal interface conductance, respectively. The nanotubes have been further characterized by X-ray photoelectron spectroscopy (XPS), Raman spectroscopy, and electron microscopy in order to account for the marked differences in electrical and thermal interface conductance.

Introduction

The extraordinary properties of carbon nanotubes (CNTs) make them promising candidates for several applications including thermal management[1,2] and electrical interconnects.[3,4] As predicted by Moore's law,[5] increased device integration and related heat dissipation present a pressing issue that necessitates the development of reliable and low-cost thermal interface materials that dissipate heat efficiently from devices to the heat sink. The thermal resistance of the interface between the chip and the heat sink is often the rate-limiting process for heat dissipation.[2] CNTs provide major advantages among materials currently in use as thermal interfaces[6−11] mainly because they are chemically stable, highly conformable in the interface, mechanically resilient, and highly conductive—the intrinsic thermal conductivity of an individual CNT at room temperature is estimated at 3000 W/mK.[12] In addition, van der Waals interactions between the compliant free CNT tips and the surface of an opposing substrate can enhance the contact area substantially.[13]

Multiwalled CNTs (MWCNTs) are preferred to single-walled CNTs (SWCNTs) for thermal management applications because they have a lower radial elastic modulus[14] that can facilitate more contact area between free CNT tips that interact through van der Waals forces with an opposing substrate. Moreover, a recent study[15] demonstrated that, at sufficiently low temperatures, thermal resistance at individual nanotube−substrate contacts can increase when the contact width becomes smaller than the dominant phonon wavelength, which is approximately 5 nm at room temperature for most crystalline solids. Given the promise that CNT-based thermal interface materials have shown,[16,17] substantial research attention has focused on the growth of well-anchored multiwalled CNT arrays for thermal management applications.

Another important property of CNTs is their large current-carrying capacity at room temperature,[18] often described as "ballistic" or "quasi-ballistic" for clean CNTs;[19] this attribute makes CNTs attractive for use as electrical interconnects in future very large-scale integrated circuits.[4] Standard interconnect materials such as Cu, Al, W, and silicides are prone to electromigration, particularly above certain current densities and temperatures, and this behavior hinders performance and reliability.[20−22] On the other hand, CNTs have been reported to carry high current densities up to 10^9-10^{10} A/cm^2 without apparent structural failure or changes in resistance at temperatures up to 250 °C for extended periods of time.[4] For VLSI interconnect applications, high-quality metallic CNTs with low electrical resistance are required. Because of the difficulty associated with the control of single-walled CNT chirality, multiwalled CNTs are preferred in these applications because they exhibit predominantly metallic conduction characteristics. MWCNTs are often accompanied by defects, which can adversely affect the electron transport properties. As discussed in greater detail by Meyyappan et al.,[23] plasma-enhanced chemical vapor deposition offers several advantages over other growth techniques; however, it typically produces CNTs with somewhat higher defect density as compared to CNTs produced by other methods. In this work, we demonstrate that the electrical resistance of CNTs can be varied, and the results reveal a mild inverse correlation between electrical resistance and CNT quality.

A unique feature of the microwave plasma chemical vapor deposition (MPCVD) process is the presence of a wide parameter space that facilitates the control of the CNT growth properties. The dc voltage bias is one of the influential parameters of the MPCVD because it directly modulates the ion flux to the substrate[24] by controlling the attraction or repulsion of ions by the substrate. In the present work, we report the electron transport properties of individual CNTs and the

* Authors to whom correspondence should be addressed. E-mail: pamama@purdue.edu (P.B.A.); tsfisher@purdue.edu (T.S.F.).
† Birck Nanotechnology Center.
‡ Department of Physics.
§ School of Mechanical Engineering.

10.1021/jp807607h CCC: $40.75 © 2008 American Chemical Society
Published on Web 11/12/2008

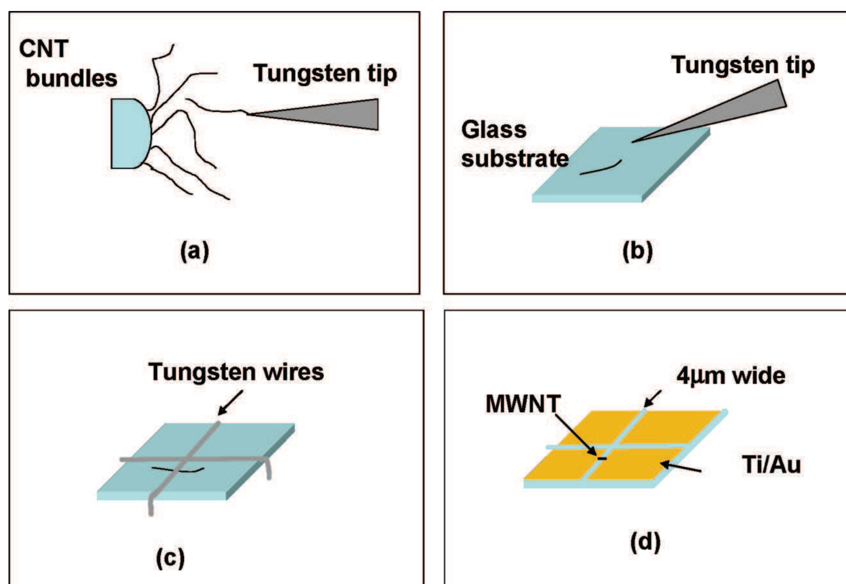

Figure 1. Schematic representation of the procedure for preparing individual CNT samples with Au/Ti electrodes for $I-V$ measurement.

thermal interface conductance of CNT arrays grown under dc bias voltages of −200, −100, 0, +100, and +200 V. Biasing the substrate positively repels H^+ and other positively charged ions generated in the plasma, thereby reducing any damage these ions might produce during nanotube growth. Conversely a negative bias attracts positive ions, increasing the likelihood of defect formation. In particular, enhanced electrical conductance and reduced thermal interface resistance of individual CNTs and CNT arrays grown under positive dc bias voltage (+200 V), respectively, have been demonstrated. Electrical resistances of individual CNTs were obtained from low-bias $I-V$ measurements of randomly selected CNTs using a previously reported technique,[25] while the thermal interface resistance of the CNT arrays was measured using a photoacoustic technique.[11] Using field emission scanning electron microscopy (FESEM), transmission electron microscopy (TEM), Raman spectroscopy, and X-ray photoelectron spectroscopy (XPS), the influence of dc bias voltage on the structural characteristics of CNTs is also correlated with the electrical and thermal interface conductance of CNTs.

Experimental Section

Catalyst Preparation. A fourth-generation, poly(amidoamine) (PAMAM) dendrimer terminated with an amine functional group (G4-NH_2) was used to deliver Fe_2O_3 nanoparticles to Ti-coated (30 nm) SiO_2/Si substrates. The Ti undelayer enhances CNT growth and promotes good adhesion of the CNT arrays to the substrate. Such adhesion is desirable in thermal interface material applications where reliability over several cycles of use is highly important. The dendrimer polymer [NH_2-$(CH_2)_2NH_2$]$(NH_2)_{64}$ was supplied as a 10% CH_3OH solution from Aldrich. The catalyst solution was prepared by mixing two solutions containing 5.56 mmol of $FeCl_3\cdot 6H_2O$ (Aldrich) and 0.12 mmol of G4NH_2 for 3 h. The catalyst solution was kept for ~48 h before it was used for nanotube growth. The G4-NH_2-templated catalyst was immobilized on cleaned Ti/SiO_2/Si substrates by dip-coating for 10 min and drying in N_2. The Ti/SiO_2/Si-supported catalyst was calcined at 550 °C for 30 min (heating rate = 30 °C/min) to remove the dendrimer, leaving a monolayer of exposed nearly monodispersed Fe_2O_3 nanoparticles.

Growth of CNTs by MPCVD. The Ti/SiO_2/Si-supported catalyst was placed on a Mo puck (5.1 cm in diameter, 3.3 mm thick) to concentrate the plasma directly above the sample, and the puck and substrate were then introduced into the microwave MPCVD reactor (SEKI AX5200S). The chamber was evacuated to 0.5 Torr by an external mechanical pump and then pressurized to 10 Torr using N_2; the temperature was increased to 900 °C in flowing N_2 (50 sccm). N_2 ambient enhances the stability of Fe_2O_3 nanoparticles in the MPCVD growth environment and preserves catalytic activity.[26] Inductive substrate heating was supplied by a 3.5 kW radio frequency power supply acting on a graphite susceptor. The substrate's surface temperature was monitored using a Williamson dual wavelength pyrometer (model 90) while a shielded K-type thermocouple located 2.5 mm below the surface of the heated graphite susceptor provided a temperature feedback control. At the reaction temperature, the gas flow was switched from N_2 to 50 sccm of H_2. After attaining steady state, the H_2 plasma was ignited using a microwave power of 200 W, and 5 sccm of CH_4 was fed into the chamber for 20 min. The chamber was evacuated and then allowed to cool to room temperature after each run.

***I−V* Measurements.** Individual CNTs were randomly selected from the as-prepared samples for this study using procedures reported by dePablo et al.[18] A schematic representation of the procedure for preparing individual CNT samples with Au/Ti electrodes is shown in Figure 1. First, we manipulated a 4 μm diameter tungsten wire on a 1.5 cm by 1.5 cm cleaned glass substrate and fixed it on both ends. A randomly selected CNT from the as-prepared sample was then mounted on a sharp tungsten tip, and was then carefully placed on the as-prepared glass substrate with the CNT parallel to the tungsten wire. A second 4 μm diameter tungsten wire was then positioned across the first wire and the CNT to serve as a mask from above. Because the first wire was already positioned on the surface, the second wire was slightly elevated so that it did not contact the underlying CNT. The entire substrate assembly was then placed into a thermal evaporator, and approximately 10−15 nm thick Ti and 50−100 nm thick Au films were evaporated on the top surfaces. After removing the tungsten wires, Au/Ti electrodes were in contact to both ends of each CNT.[18,25] A total of five individual nanotubes were studied for each growth condition (or dc bias voltage), and the nanotubes were randomly picked from three samples of MWCNT arrays grown independently. All samples studied in this work were prepared by the

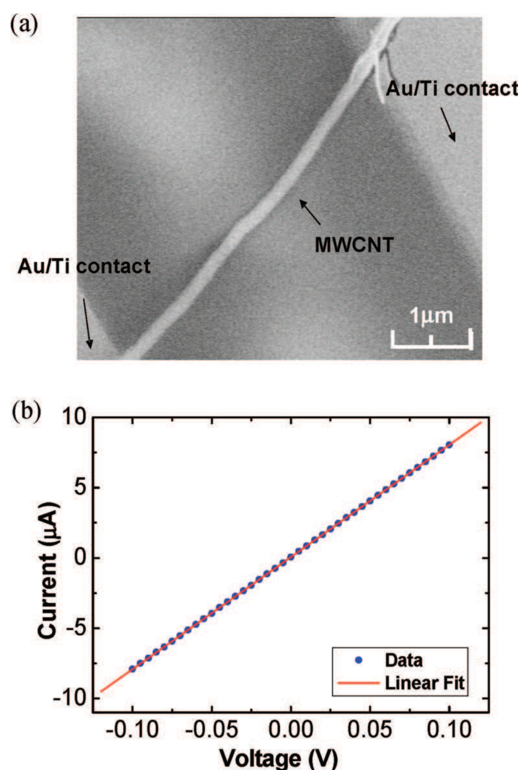

Figure 2. (a) Representative FESEM image of a CNT sample. The distance between the Au/Ti electrodes is approximately 4 μm. (b) Representative $I-V$ plot of the measured CNT samples. The red solid line is the least-squares linear fitting line. Electrical resistance of the measured CNT sample can be determined from the slope of the fitting line.

same procedure to ensure consistency and to allow quantitative comparisons among the samples. After sample preparation, a field emission scanning electron microscope (Hitachi S-4800) was used to characterize the samples, and a representative FESEM image is shown in Figure 2a.

The experimental setup for acquiring $I-V$ data of individual MWNTs consists of a Keithley 428 current amplifier, a National Instruments interconnect box, a computer system, and a sample holder. The software LabView 6.0 controlled the instruments and managed data collection. To avoid unwanted heating effects, $I-V$ measurements were constrained to low-bias conditions ($|V| \leq 0.1$ V) as shown in Figure 2b. For each individual CNT sample, 40 data points were collected between −0.1 V and 0.1 V. Each data point shown was the average of 50 measurements at the same voltage. The resistance of each individual CNT sample was determined from the slope of a least-squares fit line to the resulting $I-V$ plot.

Photoacoustic Measurements. The thermal performance of the CNT array interfaces was characterized using a photoacoustic technique (PA). For each dc bias voltage, three CNT array interfaces were independently produced and studied. In the PA technique,[11] a sinusoidally modulated fiber laser is used to periodically heat the surface of the CNT interface samples. The heated area of the sample's surface is surrounded by a sealed acoustic chamber; thus, a periodic pressure signal is produced and measured using a microphone embedded in the chamber wall. The measured pressure signal is used in conjunction with the model described in ref 11 to determine thermal interface resistance. A detailed description of the PA technique has been reported previously.[11] The transient nature of the PA technique and the analysis of many heating frequencies in a single experiment facilitate good resolution of thermal interface resistance (~1 mm^2 K/W) that is necessary to identify small changes[11] and to distinguish the thermal characteristics of different CNT array morphologies.

Electron Microscopy. A Hitachi S-4800 field emission scanning electron microscope operating at 10−20 kV was used to characterize the structural features of the CNT samples including the individual CNTs used for $I-V$ measurements. TEM images were obtained on a Philips CM200 instrument at 200 kV.

Raman and XPS Spectroscopy. The Raman spectra of the samples were acquired using a Renishaw Raman imaging microscope equipped with a 785 nm (1.58 eV) diode laser as the excitation source. The Raman spectrum for each sample was an average of three independent spectra acquired from multiple spots on the sample; three samples from independent growth runs for each dc bias voltage were analyzed in this way. The representative Raman spectrum for each dc bias voltage was an average of the three spectra.

X-ray photoelectron spectroscopy (XPS) was performed to further probe the quality of CNTs and the chemical behavior of the catalysts. XPS was carried out using a Kratos Ultra DLD spectrometer equipped with monochromatic Al Kα radiation ($h\nu$ = 1486.58 eV) and a commercial Kratos charge neutralizer. Both survey spectra and high-resolution spectra were collected at fixed analyzer pass energies of 160 and 20 eV, respectively. The element composition in the near-surface region was calculated after the subtraction of a Shirley-type background and taking into account the corresponding Scofield atomic sensitivity factors and empirically chosen attenuation function to compensate for different attenuation lengths of photoelectrons emitted from electron levels with different energies. The binding energy (BE) values are referenced to the Fermi level, and the energy scale was calibrated using the C 1s line at 284.8 eV. The XPS data were processed using the CasaXPS software.[27]

Results and Discussion

Figure 3 shows representative FESEM images of CNT samples grown under −200 (a), −100 (b), 0 (c), +100 (e), and +200 V (f); TEM images of CNTs grown under 0 V are included in Figure 3d. CNT lengths ranged from 30 to 50 μm, while average diameters were approximately 50 nm. In general, the spatial density of CNTs was more uniform across the entire substrate for samples grown under 0, +100, and +200 V. Regions with relatively poor CNT growth were observed for samples grown under negative bias, especially at −200 V. TEM images suggest that all structures are multiwalled nanotubes rather than fibers, and that they are well graphitized with hollow interiors having approximately 20 concentric carbon layers. The vertical orientation of the CNT arrays improved with increasing negative dc bias voltage; as shown in Figure 3f, growth under +200 V gave rise to more randomly oriented CNTs.

Raman spectroscopy is a reliable technique for characterizing the defect features of CNTs. Figure 4 shows the Raman spectra of CNTs grown under negative, zero, and positive dc bias voltages from Fe_2O_3 nanoparticles acquired using a 785 nm diode laser excitation. As the dc bias voltage is varied, several salient changes in spectral features were observed. The result of Lorentzian line shape analysis of the Raman spectra is also shown; this analysis is necessary because of the broad full width at half-maximum (FWHM) (>40 cm^{-1}) of the G-peak, which indicates the existence of multiple G peaks. The quality of the fit in the low-energy and high-energy tails of the D- and G-bands, respectively, is good. The assignment of the peak components of the D- and G-bands is consistent with the works

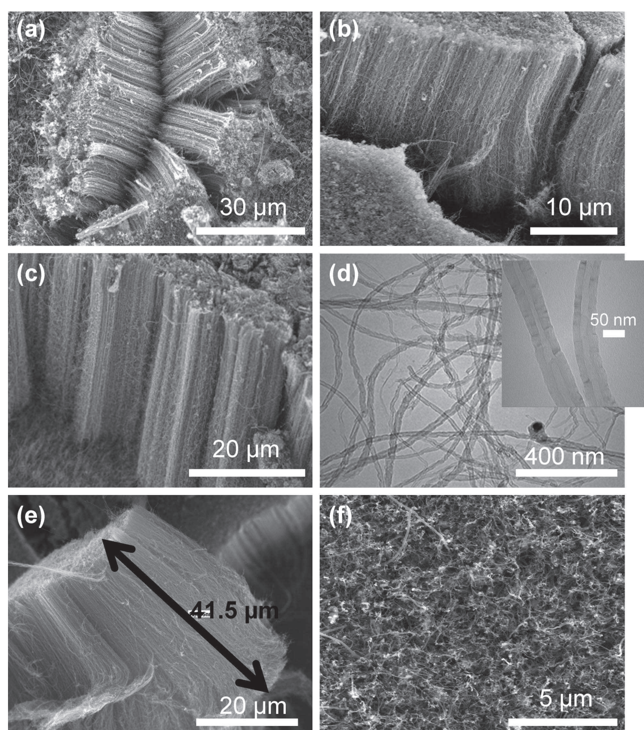

Figure 3. Morphology of CNTs grown under different dc bias voltages. FESEM images of CNTs grown under (a) −200 V, (b) −100 V, and (c) 0 V. (d) TEM images of CNTs grown under 0 V (inset shows a higher magnification image). FESEM images of CNTs grown under (e) +100 V and (f) + 200 V.

of Rao et al.[28] and Sun et al.[29] The Raman spectra are generally distinguished by two peaks around 1318 and 1595 cm^{-1} and a shoulder near 1625 cm^{-1}; the peaks are ascribed to the disorder-induced (D) mode, the C−C stretching tangential (G) mode, and the disorder-induced (D′) mode, respectively. The D′ peak is related to the maximum in the graphene 2D phonon density of states.[28,30]

As shown in Figure 4, the tangential bands for CNT samples grown under negative dc bias voltage were fitted using a Lorentzian doublet near 1596 and 1626 cm^{-1} while the D-bands were fitted with two Lorentzians at 1182 and 1321 cm^{-1}. We observed a relative increase in the D′ mode for these samples grown under negative dc bias voltage, indicating that they are of poorer quality. For CNT samples grown in the absence of dc bias voltage, the tangential bands were fitted with three Lorentzians at 1573, 1599, and 1625 cm^{-1} while the D-band was fitted with two Lorentzians at frequencies of 1181 and 1318 cm^{-1}. In the case of CNTs grown under positive dc bias voltage, their tangential bands were also resolved into three components as observed in the spectrum of CNTs grown under 0 V; however, the D-band was fitted with a single Lorentzian. The three components at 1573, 1599, and 1625 cm^{-1} correspond to the E_{2g}, E_{1g}, and A_{1g} modes, respectively;[28,29] these modes and the D-band are considered particular to the MWCNTs.[28] The peak near 1576 cm^{-1} is ascribed to vibrations in the circumferential direction, while the peak at 1584 cm^{-1} is ascribed to vibrations along the nanotube axis.[28] The peaks near 1180 cm^{-1} observed in the spectra of CNTs grown under negative and zero dc bias voltage represent sp^3 rich phases of CNTs and suggest the existence of amorphous carbon or defects on the walls of CNTs.[31] The absence of a distinct D′ mode at 1625 cm^{-1} and of a peak at 1180 cm^{-1} for CNTs grown under positive dc bias voltage indicates further that their quality is superior.

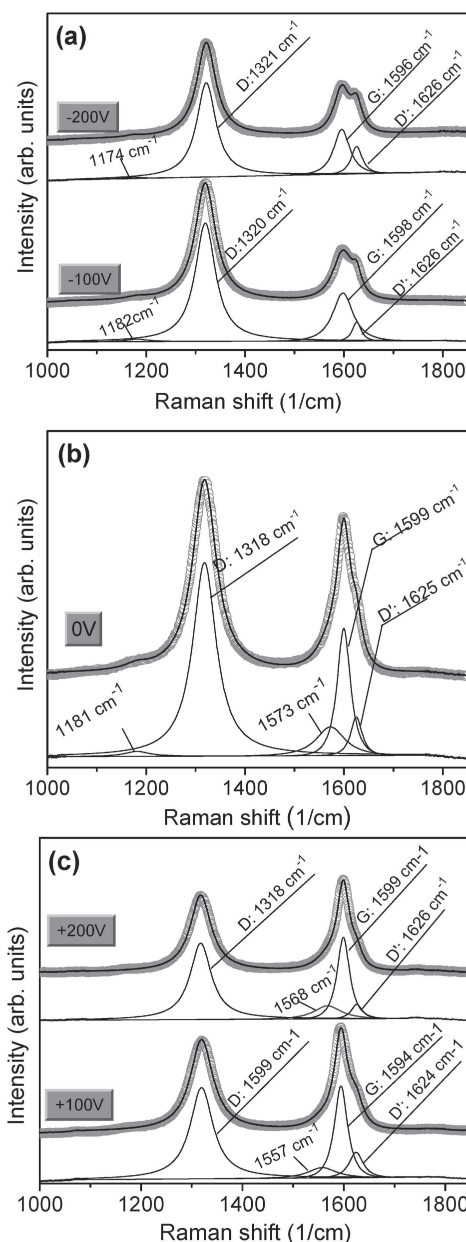

Figure 4. First order Raman modes of CNTs grown under (a) negative, (b) zero, and (c) positive dc bias voltages.

The integrated intensity of the tangential G component relative to the D component (I_G/I_D ratio), and the FWHM of the G component have been used as quality indexes to evaluate the quality of the CNTs. Yoshida et al.[32] have shown that the FWHM intensity of the G-band reflects the degree of graphitization of carbon materials. The effect of dc bias voltage on the I_G/I_D ratio and the FWHM are presented in Figure 5. The line shapes of the G- and D-bands and the quality indexes vary significantly with dc bias voltage. The I_G/I_D ratio is often affected by the CNT wall type (i.e., single-walled or multiwalled), but this factor is insignificant in this case because all CNTs observed were multiwalled. Therefore, the principal contributors to the change in the I_G/I_D ratio are expected to be the relative amount of amorphous carbon and the density of defects on the walls of the CNTs. However, as subsequently shown, the high electrical resistance of CNTs grown under negative dc bias voltage indicates that the number of defects is the dominant contributor to the I_G/I_D ratio in the present case. The highest FWHM (47.99 cm^{-1}) and the lowest I_G/I_D ratio (0.44) were observed for CNTs grown under −100 V, indicating that the number of defects

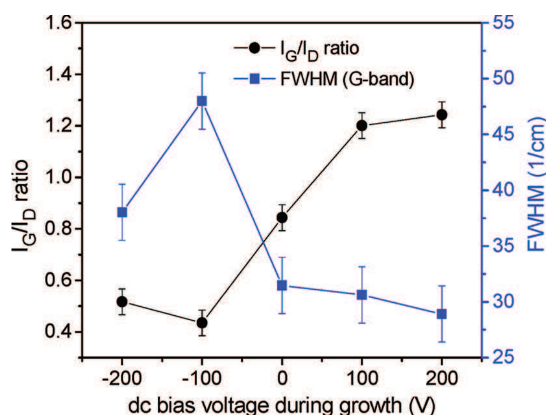

Figure 5. Integrated intensity of the G component at 1587 cm^{-1} relative to the D component at 1318 cm^{-1} (I_G/I_D ratio) and the FWHM of the G component at 1587 cm^{-1}as a function of dc bias voltage. The error bars represent standard errors of the mean values of the quality indexes.

was highest for this sample. Interestingly, a further increase in the magnitude of the negative dc bias voltage to −200 V resulted in a slight increase in the I_G/I_D ratio (0.52) and a decrease in the FWHM (38.03 cm^{-1}). Interestingly, this behavior is different from our previous results for single-walled CNTs in which increasing the magnitude of negative dc bias voltage always decreased the I_G/I_D ratio.[33]

Under increasing positive dc bias voltage (0 to +200 V), a monotonic increase and decrease in the I_G/I_D ratio and the FWHM, respectively, were observed. CNTs grown under +200 V showed the lowest FWHM (28.91 cm^{-1}) and the highest I_G/I_D ratio (1.24); this corresponds to 48% increase in the value of the I_G/I_D ratio when compared to CNTs grown in the absence of dc bias voltage. The results for both quality indexes are in good agreement.

Parts a and b of Figure 6 show the XPS survey spectra and the normalized integrated area under the XPS C 1s peak of CNTs grown under the various dc bias voltages, respectively. Because the probe depth of XPS is small (<10 nm), it is extremely difficult to detect the surface species (catalyst and underlayer) for dense CNT arrays. Samples grown under negative dc bias voltage exhibit distinct Si 2s and Si 2p peaks at binding energies near 150 and 100 eV, respectively. The presence of Si peaks for these samples suggests that the density of CNTs was lower, thereby allowing Si on the substrate to be detected. The integrated area under the C 1s peak presented in Figure 6b provides a measure of the carbon yield. We observed that the overall carbon yield increases with increasing bias voltage from negative to positive and reaches a maximum for CNTs grown under the highest positive dc bias voltage. As revealed by FESEM studies and the quality indexes presented in Figure 5, the high carbon yield observed for CNT samples grown under positive dc bias voltage confirms their higher CNT density.

A study to characterize the electrical properties of the CNTs grown under −200, −100, 0, +100, and +200 V was carried out by measuring the $I-V$ behavior of randomly selected individual CNTs. The corresponding electrical resistances obtained for each CNT sample are presented as a function of dc bias voltage during growth in Figure 7. Five CNT samples were studied for each dc bias voltage. The data indicate that CNTs grown under positive dc bias voltage exhibit the lowest resistances while the highest resistances were observed for CNTs grown under negative dc bias voltage. The $I-V$ data may contain information about the defect density present in CNTs.[25]

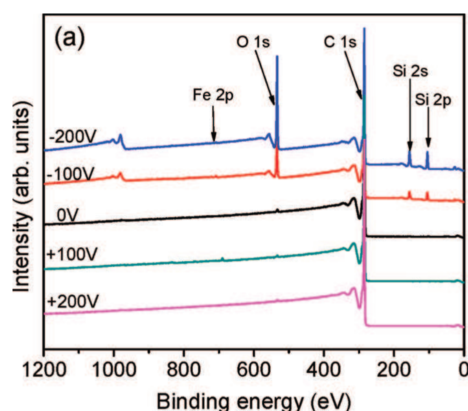

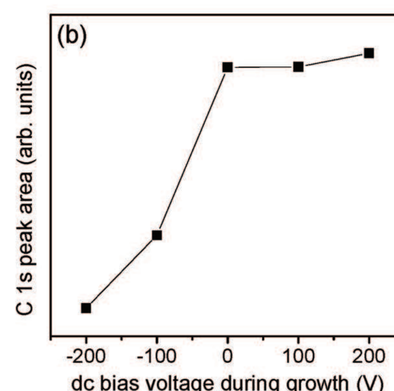

Figure 6. (a) XPS survey spectra of CNTs grown under −200, −100, 0, +100, and +200 V; (b) Normalized integrated area under the C 1s peak of CNTs, as measured by XPS, as a function of dc bias voltage.

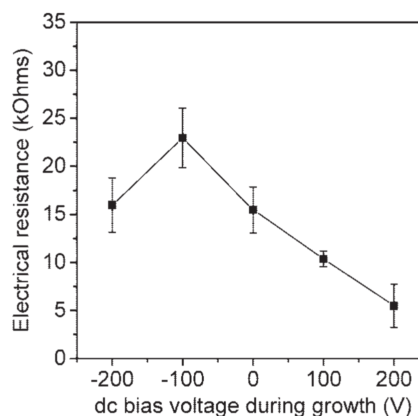

Figure 7. Measured electrical resistance of individual CNTs as a function of dc bias voltage used during growth in the MPCVD. The error bars represent standard errors of the mean values of the electrical resistance.

Consequently, it is reasonable to conclude that negative dc bias voltage produces higher defect densities on the CNTs; the effect is more pronounced for CNTs grown under −100 V, evidenced by the highest resistance (23.0 kΩ) observed. As the negative dc bias voltage magnitude increases to −200 V, the resistance decreases to 16.0 kΩ. In the case of positive dc bias voltage, resistance decreases with increasing dc bias voltage; the corresponding resistances for +100 and +200 V were 10.4 and 5.5 kΩ, respectively. Our previous study of the relationship between electrical resistance and CNT growth temperatures has shown that the quality indexes correlate well with differences in electrical resistance,[25] and the present results reveal a similar correlation, namely that lower quality indexes produce MWCNTs with consistently higher electrical resistance.

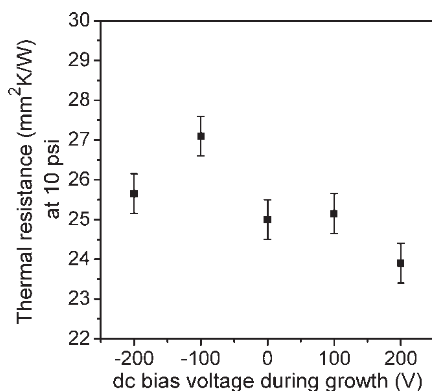

Figure 8. Measured thermal interface resistance of CNT arrays determined using a photoacoustic technique as a function of dc bias voltage used during growth in the MPCVD. The experimental uncertainty for the PA measurements is ± 0.5 mm^2 K/W.

In addition to electrical characteristics, the thermal behavior of the CNT arrays was also determined using a PA technique. Figure 8 shows the variation of thermal interface resistance of CNT arrays with the dc bias voltage applied during growth. The thermal resistance measurements were performed at a single interface pressure (69 kPa) that is typical of the pressure applied between a heat sink and a Si chip. The thermal resistance values obtained for the CNT samples are fairly comparable to those reported for CNT interfaces grown from film catalysts.[7,8,10] In general, the dependence of thermal interface resistance on the dc bias voltage reveals a trend that is somewhat analogous to that observed earlier for electrical resistance. However, because the thermal interfaces consist of arrays of CNTs (as opposed to individual tubes), the observed data trend is likely the result of more complex interactions among tube quality, diameter, and macroscopic MWCNT coverage. The lowest thermal interface resistance (24 ± 0.5 mm^2 K/W) was observed for CNT arrays grown under a dc bias voltage of +200 V, while CNT arrays grown at −100 V showed the highest thermal interface resistance (27 ± 0.5 mm^2 K/W). Although our previous results,[34] in which the CNT coverage was similar for all samples, showed that the more defective CNT arrays achieved lower thermal interface resistance, we attribute variations in thermal resistance here primarily to the effect of dc bias voltage on the macroscopic CNT coverage, which can influence the amount of real contact established in the interface.[35]

The present results suggest that dc bias voltage is an influential synthesis parameter that can be used to control the number of defects in CNTs. It is clear from Figure 7 that, to obtain high electrical conductance, CNTs should be grown under positive dc bias voltage. Biasing the substrate positively results in the repulsion of H^+ and other positively charged hydrocarbon ions generated in the plasma, thereby reducing the impingement of these ions. On the other hand, a negatively biased substrate attracts these positively charged ions to the growth substrate, thereby increasing the formation of defects.

The results presented in Figures 5 and 7 suggest that dc bias voltage may be used to control the number of defect sites on the walls of CNTs. Note that, for some applications, defects on the walls of CNTs are generated or induced by postsynthesis treatment such as aggressive sonication, and this process can be difficult to control because it depends on several factors such as sonication time, power, frequency, and the type of solvent used. The presence of defects on the walls of CNTs can benefit electroanalytical application, as defective CNTs have the ability to promote electron transfer reactions with relevant biomolecules.[36] Further, for electrochemical DNA sensing, the presence of edge planes of graphene at intervals along the walls of bamboo-structured MWCNTs resulted in superior electrochemical performance compared to SWCNTs.[37] The present results demonstrate that the density of defects present in CNTs may be controlled with high reproducibility using dc bias voltage during synthesis.

Conclusions

In this work, we have demonstrated enhanced electrical and thermal interface conductance of individual CNTs and CNT arrays grown under positive dc bias voltage (+200 V) by MPCVD. We attribute the variation in the electrical resistance of the CNTs to the differences in the quality and the surface morphology of the CNTs. The variation in the thermal interface resistance of the CNT arrays is attributed primarily to the effect of bias on macroscopic CNT coverage, which can influence the amount of real contact established in the interface. The overall carbon yield increases with decreasing negative bias voltage and reaches a maximum for CNTs grown under positive dc bias voltage. The electrical and thermal interface resistances of the CNTs tend to show a somewhat inverse correlation with the quality of the CNTs. The absence of a distinct D′ mode at 1625 cm^{-1} and a peak at 1180 cm^{-1} for the Raman spectra of CNTs grown under positive dc bias voltage suggest that their quality is superior. This work also shows that increasing the magnitude of negative dc bias voltage does not necessarily result in a corresponding decrease in the quality of CNTs; the quality of CNTs grown at −100 V decreases substantially, but it improves at −200 V. Given that the presence of defects on the walls of CNTs could be of benefit for some applications such as electrochemical biosensing, an additional outcome of this work involves the control of defect density through bias voltage during growth.

Acknowledgment. This research was supported by the NASA-Purdue Institute for Nanoelectronics and Computing, the Cooling Technologies Research Consortium (an NSF I/UCRC), and the Birck Nanotechnology Center. The authors gratefully acknowledge the assistance of Dr. Dmitry Zemlyanov in XPS analysis. B.A.C. also acknowledges Intel Foundation and Purdue University Graduate School for financial support.

References and Notes

(1) Xu, J.; Fisher, T. S. *Int. J. Heat Mass Transfer* **2006**, *49*, 1658.
(2) Shaikh, S.; Lafdi, K.; Silverman, E. *Carbon* **2007**, *45*, 695.
(3) Baughman, R. H.; Zakhidov, A. A.; deHeer, W. A. *Science* **2002**, *297*, 787.
(4) Srivastava, N.; Banerjee, K. *IEEE* **2005**, 0-7803-9254-X.
(5) Moore, G. E. IEEE, International Solid-State Circuits Conference, 2003.
(6) Cola, B. A.; Maschmann, M. R.; Henry, C.; Fisher, T. S. Proceedings of VMIC-VLSI/ULSI Multilevel Interconnect Conference, Fremont, CA.
(7) Xu, J.; Fisher, T. S. *IEEE Trans. Compon., Packag. Technol.* **2006**, *29*, 261.
(8) Hu, J. X.; Padilla, A. A.; Xu, J.; Fisher, T. S.; Goodson, K. E. *J. Heat Transfer* **2006**, *128*, 1109.
(9) Tong, T.; Zhao, Y.; Delzeit, L.; Kashani, A.; Meyyappan, M.; Majumdar, A. *IEEE Trans. Compon., Packag. Technol.* **2007**, *30*, 92.
(10) Cola, B. A.; Xu, X.; Fisher, T. S. *Appl. Phys. Lett.* **2007**, *90*, 093513.
(11) Cola, B. A.; Xu, J.; Cheng, C.; Hu, H.; Xu, X.; Fisher, T. S. *J. Appl. Phys.* **2007**, *101*, 054313.
(12) Kim, P.; Shi, L.; Majumdar, A.; McEuen, P. L. *Phys. Rev. Lett.* **2001**, *87*, 215502.
(13) Hertel, T.; Walkup, R. E.; Avouris, P. *Phys. Rev. B* **1998**, *58*, 13870.
(14) Palaci, I.; Fedrigo, S.; Brune, H.; Klinke, C.; Chen, M.; Riedo, E. *Phys. Rev. Lett.* **2005**, *94*, 175502.
(15) Prasher, R.; Tong, T.; Majumdar, A. *J. Appl. Phys.* **2007**, *102*, 104312.

(16) Liu, H.; Huang, H.; Wu, Y.; Fan, S. S. *Appl. Phys. Lett.* **2004**, *84*, 4248.

(17) Bieruck, M. J.; Llaguno, M. C.; Radosalvljevic, M.; Hyun, K. K.; Johnson, A. T.; Fischer, J. E. *Appl. Phys. Lett.* **2002**, *80*, 2767.

(18) dePablo, P. J.; Graugnard, E.; Walsh, B.; Datta, S.; Reifenberger, R. *Appl. Phys. Lett.* **1999**, *74*, 323.

(19) Frank, S.; Poncharal, P.; Wang, Z. L.; deHeer, W. A. *Science* **1998**, *280*, 1744.

(20) Hauder, M.; Gstöttner, J.; Hansch, W.; Schmitt-Landsiedel, D. *Appl. Phys. Lett.* **2001**, *78*, 838.

(21) Wei, B. Q.; Vajtai, R.; Ajayan, P. M. *Appl. Phys. Lett.* **2001**, *79*, 1172.

(22) Srivastava, N.; Banerjee, K. ICCAD, 2005.

(23) Meyyappan, M.; Delzeit, L.; Cassell, A.; Hash, D. *Plasma Sources Sci. Technol.* **2003**, *12*, 205.

(24) Yen, J. H.; Leu, I. C.; Lin, C. C.; Hon, M. H. *Appl. Phys. A: Mater. Sci. Process.* **2005**, *80*, 415.

(25) Lan, C.; Amama, P. B.; Fisher, T. S.; Reifenberger, R. G. *Appl. Phys. Lett.* **2007**, *91*, 093105.

(26) Amama, P. B.; Maschmann, M. R.; Fisher, T. S.; Sands, T. D. *J. Phys. Chem. B* **2006**, *110*, 10636.

(27) Fairley, N. *CasaXPS*, 2.3.12; 1999−2006.

(28) Rao, A. M.; Jorio, A.; Pimenta, M. A.; Dantas, M. S. S.; Saito, R.; Dresselhaus, G.; Dresselhaus, M. S. *Phys. Rev. Lett.* **2000**, *84*, 1820.

(29) Sun, H. D.; Chen, T. J.; Li, G. *Solid State Commun.* **1999**, *109*, 365.

(30) Dresselhaus, M. S.; Dresselhaus, G.; Saito, R.; Jorio, A. *Phys. Rep.* **2005**, *409*, 47.

(31) Kim, H. M.; Kim, H. S.; Park, S. K.; Joo, J.; Lee, T. J.; Lee, C. J. *J. Appl. Phys.* **2005**, *97*, 026103.

(32) Yoshida, A.; Kaburagi, Y.; Hishiyama, Y. *Carbon* **2006**, *44*, 2333.

(33) Maschmann, M. R.; Amama, P. B.; Goyal, A.; Iqbal, Z.; Fisher, T. S. *Carbon* **2006**, *44*, 2758.

(34) Amama, P. B.; Cola, B. A.; Sands, T. D.; Xu, X.; Fisher, T. S. *Nanotechnology* **2007**, *18*, 385303.

(35) Cola, B. A.; Xu, J.; Fisher, T. S. *Int. J. Heat Mass Transf.* In review.

(36) Wang, Z.; Li, M.; Shi, Z.; Li, N.; Gu, Z. *Anal. Chem.* **2002**, *74*, 1993.

(37) Heng, L. Y.; Chou, A.; Yu, J.; Chen, Y.; Gooding, J. J. *Electrochem. Commun.* **2005**, *7*, 1457.

JP807607H